Prediction of half-metallic ferrimagnetic quadruple perovskites $A\mathrm{Cu_3Fe_2Re_2O_{12}}$ (A = Ca, Sr, Ba, Pb, Sc, Y, La) with high Curie temperatures

Duo Wang,[1] Monirul Shaikh,[2] Saurabh Ghosh,[2] and Biplab Sanyal[1,*]

[1]*Department of Physics and Astronomy, Uppsala University, Box-516, 75120 Uppsala, Sweden*

[2]*Department of Physics and Nanotechnology and SRM Research Institute, SRM Institute of Science and Technology, Kattankulathur 603 203, Tamil Nadu, India*

(Received 17 November 2020; revised 10 March 2021; accepted 16 April 2021; published 11 May 2021)

A- and B-site ordered quadruple perovskites with the chemical formula $AA'_3B_2B'_2O_{12}$ can form with 1:3 ratio at the A site. A unique feature of this specially ordered perovskite is that three different atomic sites (A′, B, and B′ sites) can all accommodate magnetic transition metals. As a consequence, multiple magnetic and electronic interactions can occur at A′, B, and/or B′ sites, giving rise to a series of intriguing physical phenomena. $CaCu_3Fe_2Re_2O_{12}$ is a good example, which shows half-metallic electronic structure, large magnetization, and a very high Curie temperature. Here we investigated a series of ferrimagnetic (FiM) compounds $ACu_3Fe_2Re_2O_{12}$ (A=Ca, Sr, Ba, Pb, Sc, Y, La) by using density functional theory and Monte Carlo simulations. We found that all compounds with A^{2+} ions exhibit high Curie temperatures (above 405 K), and the compounds with A^{3+} substitution yield even higher T_C (above 502 K). By examining interatomic exchange parameters, we found that the antiferromagnetic exchange couplings between Re and Cu as well as Re and Fe are responsible for this very high Curie temperature. For the compounds with A^{3+} substitution, electron doping in bands around the Fermi level dominated by the Re ions strengthens the Re-Cu, Re-Fe, and Re-Re exchange interactions, which cause an increase in the critical temperature. Finally, we calculated the formation energies of the quadruple perovskites with respect to the possible decomposition pathways and have found that the values are reasonable for the synthesis of these compounds under the conditions of high pressure and high temperature. In summary, this work demonstrates a design strategy of enhancing the spin ordering temperature by replacing A-site nonmagnetic ions.

DOI: 10.1103/PhysRevMaterials.5.054405

I. INTRODUCTION

In the past decades, ABO_3 perovskite oxides have received much attention due to the wide variety of physical properties and fascinating functionalities such as piezoelectricity, ferroelectricity, superconductivity, colossal magnetoresistance, and multiferroicity to name a few. In order to actually utilize these properties, high phase transition temperatures close to or even above room temperature are usually required. Due to the high flexibility of the crystal structure and the AB charge combination in perovskites, extensive research has been conducted on chemical doping at the B site to design ordered perovskites with high charge and/or spin ordering temperature. Two interesting examples are the half-metallic ferrimagnetic (FiM) compounds Sr_2FeMoO_6 [1] and Sr_2FeReO_6 [2], which are B-site ordered double perovskites with $T_c = 420$, 401 K, respectively. This high T_c stimulated research on 3*d*-4*d* and 3*d*-5*d* magnetic materials with high ordering temperatures. In these two compounds, an energy gap is formed between the Fe $e_g(\uparrow)$ and $t_{2g}(\downarrow)$ bands, and the level of Mo/Re energy positioning between the Fe *d* orbitals is the reason for half-metallicity and high critical temperature. Compared to Mo-based perovskites, Re-based double perovskites are hard magnetic materials with a coercive field higher than 2 T. At the same time, the Re-based double perovskites retain the high spin polarization characteristics of the Mo-based double perovskites. The monoclinic Ca_2FeReO_6 compound has $T_c =$ 520–540 K [3–5], and the Ba_2FeReO_6 [6] and Sr_2FeReO_6 [2] are quasicubic half-metallic compounds with $T_c = 305$ and 401 K, respectively. Besides that, it is also possible to tune the property of the double perovskites by substituting A site atoms with trivalent cations. For example, experimental results show that the La^{3+} and Nd^{3+} substituted compounds give rise to a robust increase of the spin ordering temperature [7,8].

Until now, there have been few studies on the chemical substitution of A-site magnetic ions. For a B-site ordered double perovskite, if 3/4 of the A sites are substituted by a transition metal, then both A- and B-site ordered quadruple perovskite with formula $AA'_3B_2B'_2O_{12}$ can form. A uniqueness of this specially ordered perovskite is that all three atomic sites (A′, B, and B′ sites) can accommodate magnetic transition metals. Consequently, multiple electronic and magnetic interactions can occur among A′, B, and/or B′ sites, giving rise to a series of intriguing physical phenomena such as intersite charge disproportionation, charge transfer, spin-induced ferroelectricity,

*Corresponding author: Biplab.Sanyal@physics.uu.se

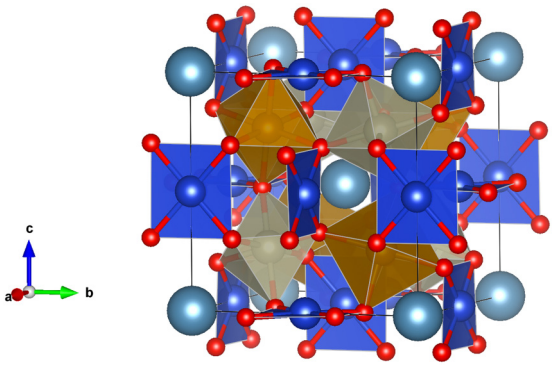

FIG. 1. Crystal structure of the parent compound $CaCu_3Fe_2Re_2O_{12}$, Ca, Cu, Fe, Re, O atoms are cyan, blue, yellow, gray, and red balls, respectively.

and FiM half-metallicity. Furthermore, it is also expected that the strong coupling between these magnetic sublattices will have an important effect on further increasing the spin or charge ordering temperature. Several compounds with this type of structure are known [9–17]. $CaCu_3Fe_2Sb_2O_{12}$ [9,10] and $CaCu_3Cr_2Sb_2O_{12}$ [11] are FiM insulators with T_c's between 160 and 170 K, in which the B′ site is occupied by nonmagnetic Sb^{5+} ions. $CaCu_3Fe_2Os_2O_{12}$ [12] is a FiM insulator with magnetic Os^{5+} ions, possessing a Curie temperature of 580 K. $CaCu_3Fe_2Re_2O_{12}$ [13] is another example which also shows a FiM ground state with high T_c (up to 560 K) but with highly spin-polarized conduction electrons. A few recent reports emerged and show large magnetization and strong magnetoelectric coupling around room temperature [13,14]. These two phenomena are highly desired for modern day technologies.

In this paper, we report a systematic investigation on quadruple perovskites, specifically the $CaCu_3Fe_2Re_2O_{12}$ and six other A-site substituted compounds with both divalent (Sr^{2+}, Ba^{2+}, Pb^{2+}) and trivalent (Sc^{3+}, Y^{3+}, La^{3+}) cations by using density functional theory (DFT) and Monte Carlo simulations. We found that all of these compounds are half metallic with FiM ground state and high Curie temperature. The use of Sr^{2+}, Ba^{2+}, and Pb^{2+} atoms for isovalent substitutions will result in moderate changes in magnetic properties through structural modifications that modify mildly the hybridization and the electronic band structure. In contrast, the electron doping by means of A^{3+} substitution gives rise to a robust increase in the Curie temperature. We analyzed the mechanism and found that a net electron doping on the band near the Fermi level, which is dominated by Re d state, plays a crucial role in increasing T_c.

II. COMPUTATIONAL METHODS

Our computational approach is based on first-principles electronic structure calculations within density functional theory (DFT) [18]. We first performed a full structural relaxation by the plane wave projector augmented wave (PAW) method [19,20], as implemented in the VASP code [21]. The plane-wave energy cutoff was set to 600 eV, and the forces were converged to 0.005 eV/Å. The k integration in the Brillouin zone was performed using $5 \times 5 \times 5$ points for geometry optimization and $7 \times 7 \times 7$ points for self-consistent calculations. The optimized structure was then used as input for the calculations of interatomic exchange parameters by means of the magnetic force theorem (MFT) [22] using full-potential linear muffin-tin orbital (FP-LMTO) code RSPT [23]. To describe the exchange-correlation effects, we used the generalized gradient approximation (GGA) [24] augmented by the Hubbard-U corrections (GGA+U) [25,26]. We performed simulations with the Coulomb U values of 8 eV, 5 eV, 2eV for the Cu-d, Fe-d, Re-d electrons, respectively, while the intra-atomic Hund's exchange parameter J was kept as 1 eV for all of them. The double counting we chose is the fully localized limit (FLL), which is an appropriate choice due to the half-metallic nature of the system. Finally, we used the extracted $J'_{ij}s$ to calculate the ordering temperatures of the compounds by means of a classical Monte Carlo (MC) algorithm for the solution of the Heisenberg Hamiltonian as implemented in the UPPASD code [27]. In our simulations, the size ranges from $5 \times 5 \times 5$ (5000 atoms) to $12 \times 12 \times 12$ (69 120 atoms). Also, periodic boundary condition and five ensembles are used to properly average the properties.

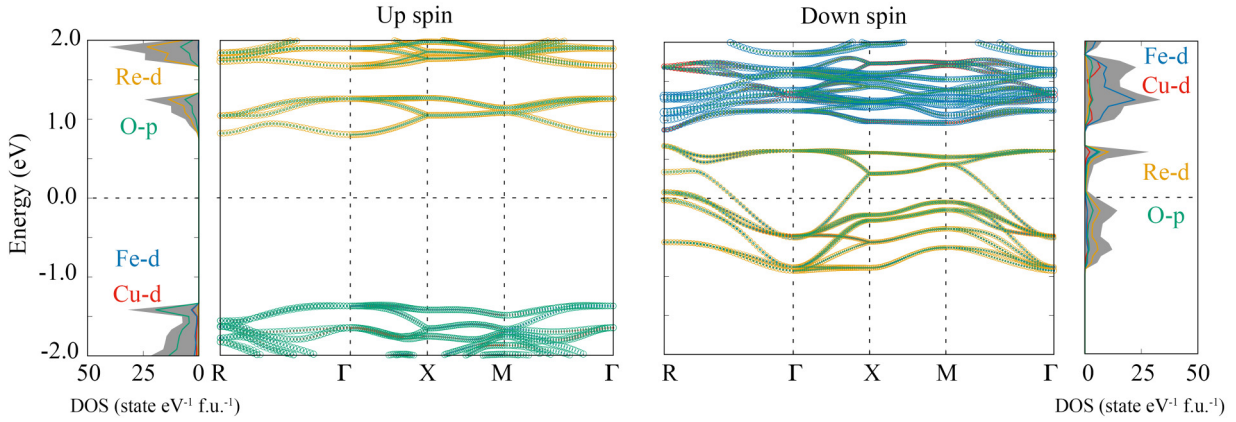

FIG. 2. Density of states (DOS) and projected band structure for up-spin and down-spin electrons of $CaCu_3Fe_2Re_2O_{12}$. Total DOS (shaded regions) and partial DOS of Cu (red curves), Fe (blue curves), Re (yellow curves) and O (green curves) are shown. The size of circles in the band structure is proportional to the weight.

TABLE I. Magnetic moments, unit in μ_B.

		A	Cu	Fe	Re	O	Total
A^{2+}	Ca	−0.023	0.632	4.090	−0.985	0.103	9
	Sr	−0.023	0.624	4.101	−0.979	0.105	9
	Ba	−0.035	0.616	4.095	−0.968	0.107	9
	Pb	−0.029	0.629	4.108	−0.995	0.106	9
A^{3+}	Sc	−0.096	0.592	4.089	−1.249	0.095	8
	Y	−0.038	0.606	4.084	−1.270	0.092	8
	La	−0.058	0.621	4.079	−1.262	0.090	8

III. RESULTS AND DISCUSSIONS

A. Crystal structure and stability

The crystal structure of the quadruple perovskite compound $CaCu_3Fe_2Re_2O_{12}$ is shown in Fig. 1. Ca and Cu ions are ordered in a 1:3 ratio at the A site, which keeps twelvefold coordination as in an ideal cubic ABO_3. A′ site has four short A′-O bond lengths and four long A′-O bond lengths. The four short A′-O bond lengths form square-planar coordination. Fe and Re ions are arranged in a rock-salt-type at the B sites of the ABO_3 perovskite structure, forming the heavily tilted ReO_6 and FeO_6 octahedra with Pn-3 space group symmetry.

To determine the magnetic ground state, we did calculations with different initial magnetic configurations, and the result shows that the ground state is FiM $Ca^{2+}Cu_3^{2+}(\uparrow)Fe_2^{3+}(\uparrow)Re_2^{5+}(\downarrow)O_{12}$. The electronic structure is shown in Fig. 2. The minority down spin bands cross the Fermi level, while the majority up spin bands exhibit a band gap of 2.2 eV. Spins from the Fe^{3+} ($3d^5$, $S = 5/2$), Cu^{2+} ($3d^9$, $S = 1/2$), and Re^{5+} ($5d^2$, $S = 1$) ions all contribute to the magnetization of the compound. The values of the ionic magnetic moments (shown in Table I) are slightly lower than their ideal values due to strong hybridization with O-2p orbitals.

Consistent with the previous analysis [28], in $CaCu_3Fe_2Re_2O_{12}$, Cu^{2+} has a localized hole in its b_{1g} orbital, Re^{5+} has partially-filled t_{2g} orbitals, and Fe^{3+} is fully polarized with a half-filled 3d shell. As shown in Fig. 2, the electronic states near the Fermi level are dominated by the Re-5d orbitals, which hybridize with the Fe-3d and O-p orbitals. It is easily seen that the Re d up spin state is pushed up, and the Re d down spin state is pushed further down by hybridization with Fe and O states. These opposite movements of the Re up and down states increase the energy separation between these two states, therefore substantially increasing the effective exchange splitting at the Re site. The half-metallic nature is caused by a Fe d-O 2p-Re d hybridization, which results in a partially filled down-spin band and the Fermi level positioned in the gap of the up-spin channel [29–31].

It should be noted that spin-orbit interaction does not significantly modify the results. This produces only small changes in the spin moments to 0.600, 4.199, and −1.119 μ_B for Cu, Fe, and Re, respectively, with the same total moment of 9 $\mu_B/f.u.$ Besides that, we also compared the electronic structures from calculations with and without spin-orbit interaction, and the results are quite similar.

By changing the ionic content at the A site, two physical parameters that are important for FiM interaction can be modified in a controlled manner. One is the spatial pressure at the A site, which can be used to adjust the structural parameters, which may affect the magnetic interactions. The other one is the Fermi level electron population at the Fermi level, which is mainly contributed by the Re-O-Fe hybrid subbands responsible for the indirect FiM coupling. The crystal structure of the compound depends on the size of the A-site atom, but it is different from the double perovskite A_2FeReO_6; the Ca- and Cu-site 1:3 ratio ordered structure makes the crystal structure fixed as a cubic shape. The information about the bond length, bond angle, and volume are listed in Table II. The average atomic radius at the A site (r_A) provides continuous parameters to adjust the cationic element in the $ACu_3Fe_2Re_2O_{12}$ quadruple perovskite. For the A^{2+} substitution (Ca^{2+}, Sr^{2+}, and Ba^{2+}), when the decreasing r_A in the compound, the progressive bending of the Fe-O-Re angle, and decreasing of $d_{B(B')\text{-}O}$ bond length happened, and it causes the increase of magnetic moment on Re atoms (from 0.968 to 0.985 μ_B). As shown in Fig. 3, this minimal change in crystal structure does not affect the band structure, especially for the bands around the Fermi level. For the A^{3+} (Sc^{3+}, Y^{3+}, and La^{3+}) substitution, the decreasing r_A causes the increase of magnetic

TABLE II. Bond angle, bond length, and volume of $ACu_3Fe_2Re_2O_{12}$ (A=Ca, Sr, Ba, Pb, Sc, Y, La).

		Bond angle (°)			Bond length (Å)				Volume (Å^3)
		Re-O-Cu	Re-O-Fe	Fe-O-Cu	A-O	Cu-O	Fe-O	Re-O	
A^{2+}	Ca	111.11	140.01	108.00	2.646	1.989	2.041	1.965	426.89
	Sr	111.36	140.15	107.92	2.679	1.998	2.055	1.970	433.35
	Ba	111.83	140.23	107.74	2.736	2.012	2.079	1.978	444.41
	Pb	111.63	140.07	107.95	2.705	1.999	2.064	1.973	437.02
A^{3+}	Sc	110.10	139.45	108.33	2.579	1.985	2.021	1.977	421.75
	Y	110.31	139.60	108.35	2.607	1.993	2.032	1.983	427.93
	La	110.80	139.82	108.34	2.658	2.002	2.050	1.989	436.62

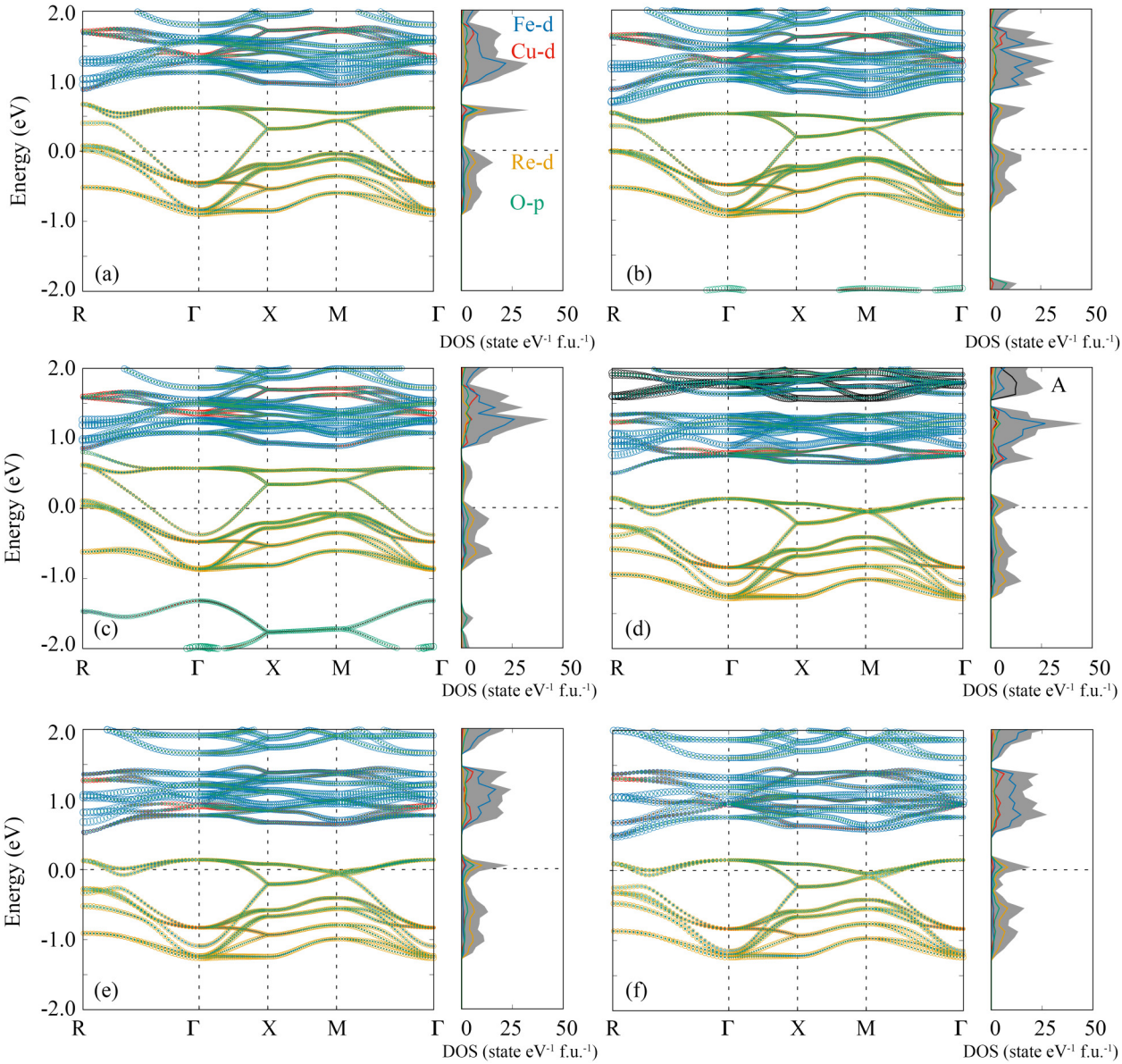

FIG. 3. Density of states (DOS) and projected band structure of $ACu_3Fe_2Re_2O_{12}$ A=Sr (a), Ba (b), Pb (c), Sc (d), Y (d), and La (f), spin down channel. Total DOS (shaded regions) and partial DOS of Cu (red curves), Fe (blue curves), Re (yellow curves), and O (green curves) are shown. The size of circles in the band structure is proportional to the weight.

moment on Fe atoms (from 4.079 to 4.089 μ_B). There is also a slight volume change because of different ionic radius of A-site cation. In addition, the electron doping is achieved in quadruple perovskites replacing divalent cations by trivalent cations at the A site. It can be easily observed in Figs. 3(d)–3(f) that a net electron doping at the Fermi level takes place with an increase in the DOS at the Fermi level. As shown in Table I, this electron doping causes a significant change in the magnetic moment at Re ions (from 0.95 to 1.22 μ_B), which corresponds to the band filling of the Re spin-down channel. The raising occupation of the Re(Fe)t_{2g} spin down subband, responsible for the hybridization and exchange mechanism, which is also beneficial for the stabilization of FiM at a higher temperature, which will be demonstrated in Sec. B.

It is worth mentioning that the parent compound and compounds with Sr^{2+}, Ba^{2+}, Sc^{3+}, Y^{3+}, and La^{3+} substitution have an energy gap in the spin-down channel. Therefore, it is expected that proper electron doping may adjust the spin and electronic properties of the present high-T_c FiM half-metal to transform to an insulator. On the contrary, for the compound with Pb^{2+} substitution, the insulating state cannot be achieved by a similar electron doping. Actually, when the Re is replaced by Os, an insulating behavior is observed in the $CaCu_3Fe_2Os_2O_{12}$ compound [9].

In order to understand the effect of structural distortion on magnetism, we performed additional structural analysis. A chemically synthesized $CaCu_3Fe_2Re_2O_{12}$ quadruple perovskite oxide with space group *Pn*-3 as low symmetry structure was considered. We obtained an idealized high symmetry structure *Pn*-3*m* where no lattice distortions are present [32]. In the subsequent step, we performed phonon calculations taking high symmetry structures and found different

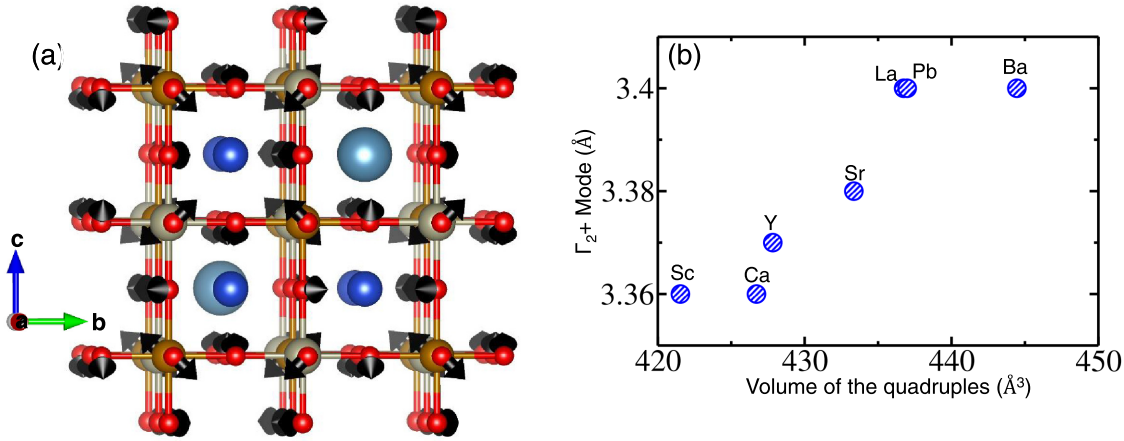

FIG. 4. (a) The most contributing mode, i.e., Γ_2^+ mode obtained from phonon calculation, Ca, Cu, Fe, Re, and O atoms are shown in cyan, blue, yellow, gray, and red colors, respectively. (b) The Γ_2^+ mode amplitude variation has been depicted as a function of increasing volume of the low symmetry structure for different A sites.

distortions that lead to different space group symmetry. Our analysis showed that, out of all modes, Γ_2^+ mode is having the maximum mode amplitude. Contribution from all other modes are negligible. Further, we found that the Γ_2^+ mode vectors are directed towards smaller A atoms, as shown in Fig. 4(a), that results in heavily tilted BO_6 and $B'O_6$ octahedra in the quadruple perovskite framework. Here, we would like to point out that in the case of transition metal oxides (TMO) of the form ABO_3, the distortions associated with BO_6 octahedra in general appear at the zone boundary. Interestingly, in the case of quadruple systems studied here, the tilt distortion responsible for phase transition appears at the zone center Γ_2^+, which is rare. The polar distortion also appears at the zone center. Thus, in this set of materials, the coupling between polar distortion which drives ferroelectricity and the tilt distortion which drives magnetism can lead to strong magnetoelectric coupling.

To have a greater insight in the participating phonon modes in the A-site ordered $Ca^{2+}Cu_3^{2+}Fe_2^{3+}Re_2^{5+}O_{12}$ quadruple perovskites and to confirm if any additional mode is playing a pivotal role in the structural phase transition, we considered other A-site cations. In a few cases only the A-sites ionic radii are varied like Sr^{2+}, Ba^{2+}, and Pb^{2+} and for a few cases we changed both ionic radii as well as their charge states such as Sc^{3+}, Y^{3+}, and La^{3+}. Altering the charge state in A site from 2+ to 3+ refers to an extra electron doping into the system. Once we obtained the full relaxed structure of individual combination in the low symmetry, we took the corresponding lattice parameters. Then we found out correct lattice parameters for high symmetry structures to avoid any unexpected strain mode for the structural phase transitions. Finally, we have performed phonon calculations taking respective high symmetry structure of quadruple perovskite oxides with the A-site substitution. We found that in both the cases there is no new contributing phonon mode. The mode amplitude of Γ_2^+ got modified with the A-site substituted $A^{2+/3+}Cu_3^{2+}Fe_2^{3+}Re_2^{5+}O_{12}$ quadruple perovskite oxides. We further observed that Γ_2^+ mode amplitude has increased moderately with the increase in volume as shown in Fig. 4(b). We infer that La, Pb, and Ba substitution will lead to more distorted structures and can have pronounced effect on the local exchange interactions.

Before going into the detailed study of magnetism we have discussed formation energy of the quadruple perovskites. The stability of a compound is one of the fundamental and important concerns when considering its application prospective. In order to study the stability of the quadruple perovskite oxides, we conducted an elaborate and extensive study to estimate the respective formation energies of the compounds. We considered various stable oxides that are associated with our quadruple perovskite oxides and were reported in the inorganic crystal structure database (ICSD) [33] (see Table I of the Supplemental Material [34]). Then we performed complete relaxation calculations for all stable oxides and considered

TABLE III. Formation energies of the quadruple perovskite systems.

Quadruple systems	Formation energies (eV/perovskite f.u.)
$CaCu_3Fe_2Re_2O_{12}$	0.624
$SrCu_3Fe_2Re_2O_{12}$	0.638
$BaCu_3Fe_2Re_2O_{12}$	2.053
$PbCu_3Fe_2Re_2O_{12}$	1.016
$ScCu_3Fe_2Re_2O_{12}$	1.490
$YCu_3Fe_2Re_2O_{12}$	1.020
$LaCu_3Fe_2Re_2O_{12}$	2.178

TABLE IV. Coordination number of each coupling as a function of distance.

	1st	2nd	3rd	4th	5th
Re-Re	12	6	24	12	
Re-Cu	6	18	18	24	36
Re-Fe	6	8	24	30	
Fe-Cu	6	18	18	24	36
Fe-Fe	12	6	24	12	
Cu-Cu	4	8	8	6	16

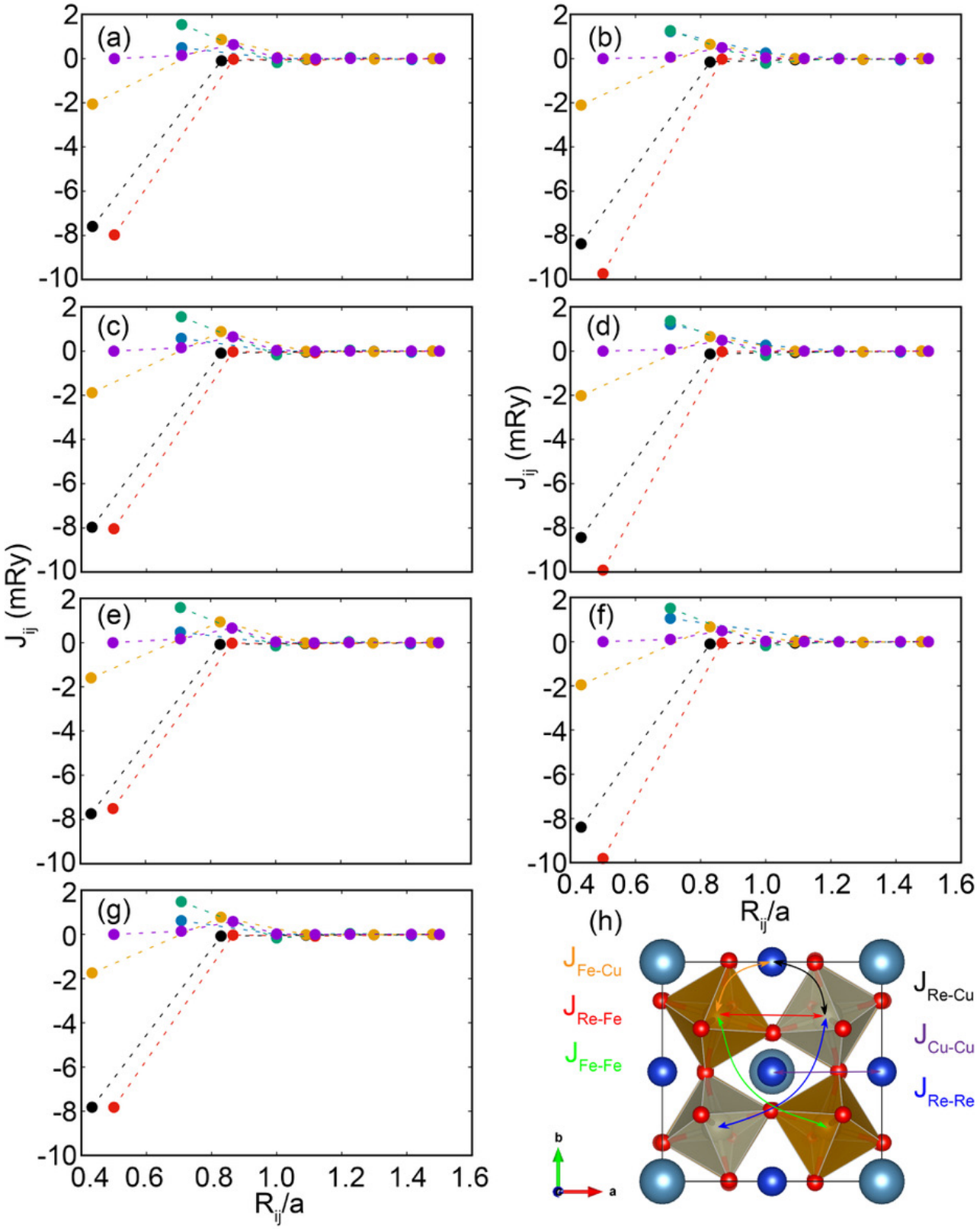

FIG. 5. Magnetic exchange parameters as a function of neighboring distance for $ACu_3Fe_2Re_2O_{12}$, A=Ca (a), Sc (b), Sr (c), Y (d), Ba (e), La (f), Pb (g). Positive values indicate FM interaction while negative values indicate AFM interaction. (h) The crystal structure as well as the identification of magnetic pair exchange are shown.

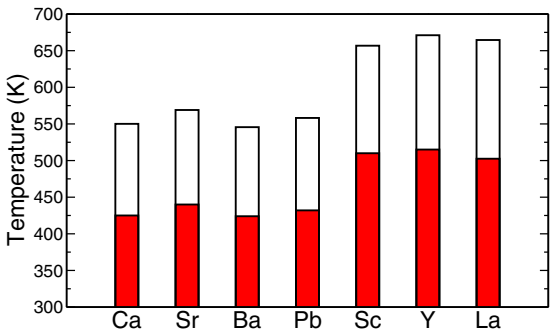

FIG. 6. Curie temperatures of $ACu_3Fe_2Re_2O_{12}$, A=Ca, Sr, Ba, Pb, Sc, Y, La calculated by mean field approximation (empty bar) and Monte Carlo simulations (filled red bar).

only the ferromagnetic arrangement of the spins for magnetic compounds within the GGA+U framework. For magnetic cations such as Cu, Fe, and Re, we used the same U values as are used for the quadruple perovskite systems. After that, we employed various combinations of stable oxides that minimize the energy of the mixture by using a linear programming problem clubbed with the grand canonical approach [35,36]. The detailed methodology of formation energy calculations are supplied in the Supplemental Material and here we have discussed the main results.

The minimum energy reaction path for Ca and Pb based quadruple perovskite systems is found to be the same and given as

$$\begin{aligned}\Delta_f E_1[A_{0.25}Cu_{0.75}Fe_{0.5}Re_{0.5}O_3] \\ = E[A_{0.25}Cu_{0.75}Fe_{0.5}Re_{0.5}O_3] - \left(\tfrac{1}{4}E[AO]\right. \\ \left. +\tfrac{3}{4}E[CuO] + \tfrac{1}{2}E[FeO] + \tfrac{1}{2}E[ReO_3]\right) \end{aligned} \quad (1)$$

with A = Ca and Pb. The minimum energy reaction path for a Ba based quadruple perovskite system is

$$\begin{aligned}\Delta_f E_2[Ba_{0.25}Cu_{0.75}Fe_{0.5}Re_{0.5}O_3] \\ = E[Ba_{0.25}Cu_{0.75}Fe_{0.5}Re_{0.5}O_3] - \left(\tfrac{1}{8}E[Ba_2ReO_5]\right. \\ \left. +\tfrac{3}{4}E[CuO] + \tfrac{1}{2}E[FeO] + \tfrac{3}{8}E[ReO_3]\right) \end{aligned} \quad (2)$$

and the minimum energy reaction paths for Sr, Sc, Y, and La based quadruple perovskite systems are

$$\begin{aligned}\Delta_f E_3[A_{0.25}Cu_{0.75}Fe_{0.5}Re_{0.5}O_3] \\ = E[A_{0.25}Cu_{0.75}Fe_{0.5}Re_{0.5}O_3] - \left(\tfrac{1}{4}E[ACuO_2]\right. \\ \left. +\tfrac{1}{2}E[CuO] + \tfrac{1}{2}E[FeO] + \tfrac{1}{2}E[ReO_3]\right) \end{aligned} \quad (3)$$

with A = Sr, Sc, Y, and La. The computed formation energies of all the quadruple perovskite oxides are shown in Table III. The formation energies are found to be positive and are in the same order of magnitude as reported in a recent study on double perovskites [36]. The quadruple perovskite systems generally synthesized at high temperature (∼1400 K) and high pressure (∼10 GPa) [13]. Thus, we believe by high pressure and/or temperature the predicted quadruple perovskites can be synthesized.

B. Magnetic exchange interaction and Curie temperature

We performed the calculations of the interatomic magnetic exchange interaction parameters as a response to the small angle tilting of spin rotation within the so-called 'magnetic force theorem.' Since the exchange between the atomic magnetic moments dictates their thermal behavior, we also performed Monte Carlo simulations based on the Metropolis algorithm and the classical Heisenberg Hamiltonian and obtained the magnetic transition temperatures.

Our results are summarized in Fig. 5 in which the nth neighbor interaction J is defined as the sum of all pairs of exchange parameters reflecting the corresponding coordination number in Table IV. There are six different intersite exchange couplings ($J_{\text{Re-Cu}}$, $J_{\text{Re-Fe}}$, $J_{\text{Re-Re}}$, $J_{\text{Fe-Cu}}$, $J_{\text{Fe-Fe}}$, and $J_{\text{Cu-Cu}}$, respectively) in the compound by introducing the A′-site Cu^{2+} ions. Two of them always make majority contributions to magnetic interaction in the system: They are the nearest $Re^{5+}(\downarrow)Cu^{2+}(\uparrow)$ and the nearest $Re^{5+}(\downarrow)Fe^{3+}(\uparrow)$; the sign of these exchange parameters is consistent with the FiM ground state ($CaCu_3(\uparrow)Fe_2(\uparrow)Re_2(\downarrow)O_{12}$). For $Fe^{3+}(\uparrow)Cu^{2+}(\uparrow)$ interaction, they are −1.027 mRy for the nearest Fe-Cu atoms and 0.432 mRy for the second nearest for the parent compound. It indicates slight magnetic frustrations because of the $Cu(\uparrow)Fe(\downarrow)$ AFM interaction. However, it is the much stronger $Re^{5+}(\downarrow)Cu^{2+}(\uparrow)$ and $Re^{5+}(\downarrow)Fe^{3+}(\uparrow)$ AFM exchange interactions that dominate the weaker $Fe^{3+}(\downarrow)Cu^{2+}(\uparrow)$ interaction and lead to the $Cu^{2+}(\uparrow)Fe^{3+}(\uparrow)Re^{5+}(\downarrow)$ long-ranged FiM spin order. Another contribution comes from the $Fe^{3+}(\uparrow)Fe^{3+}(\uparrow)$ coupling, which is 0.770 mRy for the nearest neighbor pair. It should be noted that all exchange parameters decrease to zero drastically, when the distance between atoms is bigger than the unit cell's lattice constant($x > 1$). Compared to the double perovskite A_2FeReO_6, two exchange couplings introduced by the A′-site ion ($J_{\text{Re-Cu}}$ and $J_{\text{Fe-Cu}}$) make big contributions to the magnetic interactions in the compound, which is the reason for the increased T_c in the quadruple perovskite compounds. Our calculated critical temperature from Monte Carlo simulation for the parent compound is 425 K.

For the compounds with A^{2+} substitution, there are small changes in the exchange interaction. If we consider Sr^{2+} substituted compound as an example, the nearest $Re^{3+}(\downarrow)Cu^{2+}(\uparrow)$ and the nearest $Re^{3+}(\downarrow)Fe^{3+}(\uparrow)$ interactions have increased (from 7.60 to 7.97 mRy, and from 7.98 to 8.04 mRy, respectively). The antiferromagnetic interaction between the first nearest $Fe^{3+}(\uparrow)Cu^{2+}(\uparrow)$ ions becomes weaker (from 2.05 to 1.88 mRy). Consequently, these changes increase the T_c from 425 to 440 K.

On the contrary, for the compounds with A^{3+} substitution, there are two obvious changes along with the important electron doping on Re ions. Firstly, the two most dominant exchange parameters $Re^{5+}(\downarrow)Cu^{2+}(\uparrow)$ and $Re^{5+}(\downarrow)Fe^{3+}(\uparrow)$ become stronger. Compared to the parent compound, these two $J'_{ij}s$ have increased from 7.60 to 8.38 mRy, and 7.98 to 9.72 mRy in the Sc^{3+} substituted compound. Secondly, the $Re^{3+}(\downarrow)Re^{5+}(\downarrow)$ interaction also increased from the 0.50 mRy to 1.22 mRy. Both of these changes indicate an essential effect due to the net electron doping on Re atom, which causes the robust increase in the Curie temperature as shown in Fig. 6 (T_c has increased around 80 K). This is a promis-

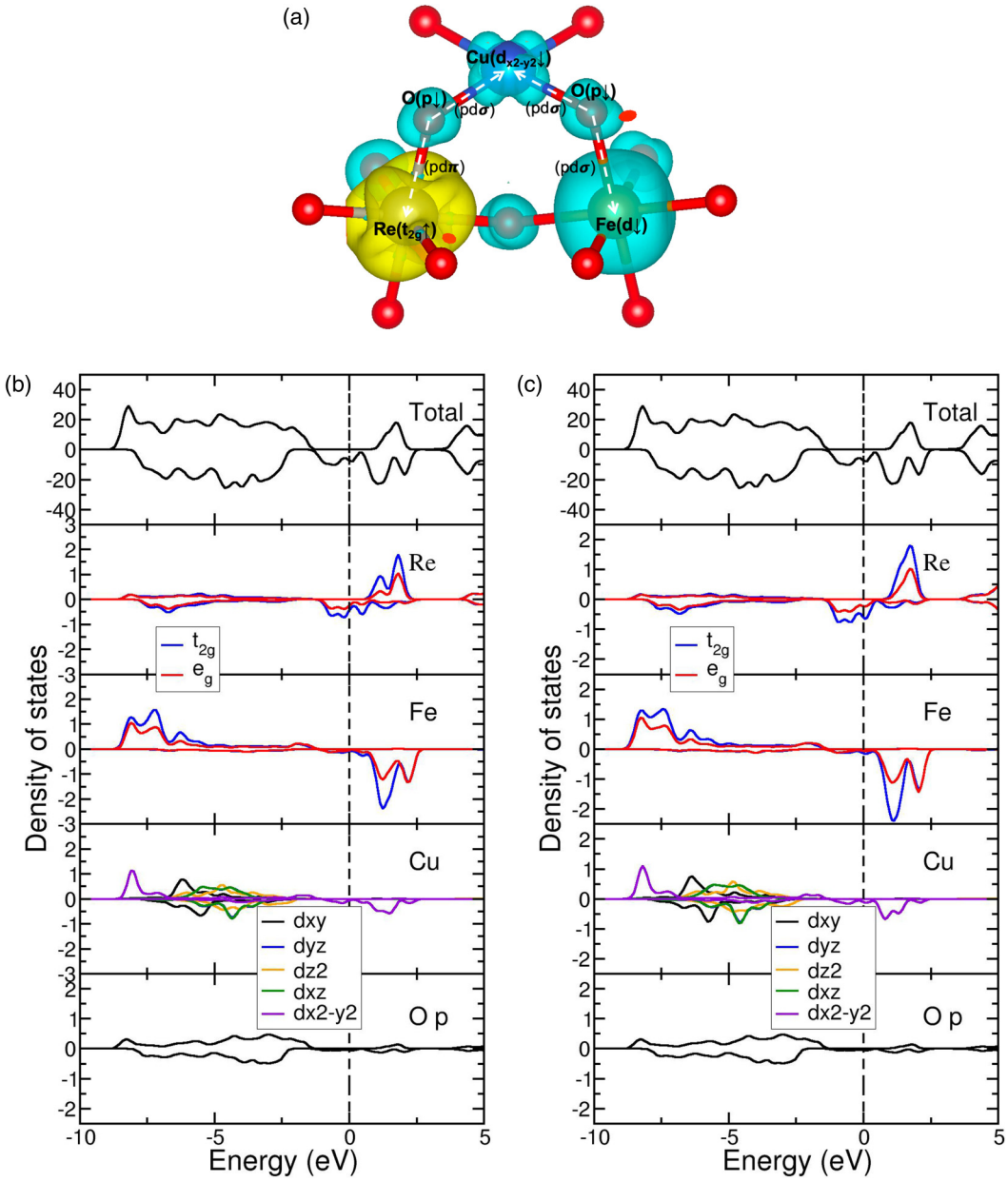

FIG. 7. Magnetization density of the parent compound CCFRO for the Cu($d_{x^2-y^2}$)-O(p)-Fe(d) and Cu($d_{x^2-y^2}$)-O(p)-Re($t2g$) band within energy range from the Fermi level to 2.5 eV. Spin magnetization is described by surface coloring (a); yellow and cyan regions present up- and down-spin polarized charge density, respectively. Calculated density of states for the parent compound (b) and the Y-substituted compound (c). The data for Re, Fe, and Cu are based on their respective local basis. Fermi level is set to zero.

ing result regarding application of these materials at room temperature and above. For comparison, we also calculated magnetic ordering temperatures by mean field approximation. As expected, the values are higher than those obtained from Monte Carlo simulations. However, the trend of temperature change is exactly the same.

To understand the mechanisms of the magnetic exchange coupling between Re, Fe, and Cu, the orbitally-resolved partial DOS for Re, Fe, Cu, and O projected in the local basis are shown in Fig. 7. Cu($d_{x^2-y^2}$), O(p), Fe(d), and Re(d) orbitals are hybridized in the energy region up to 2.5 eV above the Fermi level. For the Re atom, the t_{2g} orbitals give a major contribution to the hybridization, while for the Fe atom, both t_{2g} and e_g orbitals contribute. This situation is clearly illustrated in Fig. 7(a), which shows hybridized spin-down (cyan) Cu($d_{x^2-y^2}$), O(p), Fe(d) bands, and spin-up (yellow) Re(t_{2g}) orbitals. This also demonstrates the important role of Re(t_{2g}) orbitals as the net electron doping is mainly reflected in the t_{2g} orbitals, which is in agreement with Ref. [10].

IV. CONCLUSION

In summary, a series of quadruple perovskites $ACu_3Fe_2Re_2O_{12}$ (A=Ca, Sr, Ba, Pb, Sc, Y, La) have

been investigated by density functional theory and Monte Carlo simulations. We found that all of these compounds are stable half-metallic ferrimagnets with high Curie temperatures (above 405 K). It is noteworthy that electron doping introduced by the A^{3+} substitution yields even higher T_c (above 502.5 K). By examining crystal structures and exchange parameters, we demonstrated that the net doping on the Re-t_{2g} orbitals around the Fermi level plays a critical role. Our study shows the advantage of both A- and B-site ordered $ACu_3Fe_2Re_2O_{12}$ in a quadruple perovskite structure compared to B-site-only ordered double perovskite A_2FeReO_6 in terms of the sharp enhancement of the FiM ordering temperatures. This design strategy can be useful for realizing new magnetic materials for spintronic applications at room temperature and above.

ACKNOWLEDGMENTS

B.S. acknowledges financial support from the project grant (2016-05366) and the Swedish Research Links programme grant (2017-05447) from Swedish Research Council. D.W. thanks the China scholarship council for financial support (No. 201706210084). B.S. and D.W. gratefully acknowledge supercomputing time allocation by the Swedish National Infrastructure for Computing (SNIC) and PRACE DECI-15 project DYNAMAT. M.S. acknowledges INSPIRE division of Department of Science and Technology, Govt. of India for his fellowship. S.G. thanks DST-SERB Core Research Grand File No. CRG/2018/001728 for funding the project. M.S. and S.G. thank High Performance Computing Center, SRM IST, Chennai, India for providing the computational resources.

[1] K.-I. Kobayashi, T. Kimura, H. Sawada, K. Terakura, and Y. Tokura, Nature (London) **395**, 677 (1998).

[2] K.-I. Kobayashi, T. Kimura, Y. Tomioka, H. Sawada, K. Terakura, and Y. Tokura, Phys. Rev. B **59**, 11159 (1999).

[3] W. Westerburg, O. Lang, C. Ritter, C. Felser, W. Tremel, and G. Jakob, Solid State Commun. **122**, 201 (2002).

[4] E. Granado, Q. Huang, J. W. Lynn, J. Gopalakrishnan, R. L. Greene, and K. Ramesha, Phys. Rev. B **66**, 064409 (2002).

[5] J. M. De Teresa, D. Serrate, J. Blasco, M. R. Ibarra, and L. Morellon, Phys. Rev. B **69**, 144401 (2004).

[6] C. Azimonte, J. C. Cezar, E. Granado, Q. Huang, J. W. Lynn, J. C. P. Campoy, J. Gopalakrishnan, and K. Ramesha, Phys. Rev. Lett. **98**, 017204 (2007).

[7] P. Majewski, S. Geprägs, A. Boger, M. Opel, L. Alff, and R. Gross, J. Magn. Magn. Mater. **290**, 1154 (2005).

[8] S. Geprägs, P. Majewski, R. Gross, C. Ritter, and L. Alff, J. Appl. Phys. **99**, 08J102 (2006).

[9] W.-T. Chen, M. Mizumaki, T. Saito, and Y. Shimakawa, Dalton Transactions **42**, 10116 (2013).

[10] H. Fujii, M. Toyoda, H. Momida, M. Mizumaki, S. Kimura, and T. Oguchi, Phys. Rev. B **90**, 014430 (2014).

[11] S.-H. Byeon, S.-S. Lee, J. B. Parise, P. M. Woodward, and N. H. Hur, Chem. Mater. **17**, 3552 (2005).

[12] H. Deng, M. Liu, J. Dai, Z. Hu, C. Kuo, Y. Yin, J. Yang, X. Wang, Q. Zhao, Y. Xu *et al.*, Phys. Rev. B **94**, 024414 (2016).

[13] W.-t. Chen, M. Mizumaki, H. Seki, M. S. Senn, T. Saito, D. Kan, J. P. Attfield, and Y. Shimakawa, Nat. Commun. **5**, 3909 (2014).

[14] D. Orobengoa, C. Capillas, M. Aroyo, and J. Perez-Mato, J. Appl. Crystallogr. **42**, 820 (2009).

[15] M. S. Senn, W.-T. Chen, T. Saito, S. García-Martín, J. P. Attfield, and Y. Shimakawa, Chem. Mater. **26**, 4832 (2014).

[16] Z. Liu, X. Wang, X. Ye, X. Shen, Y. Bian, W. Ding, S. Agrestini, S.-C. Liao, H.-J. Lin, C.-T. Chen, S.-C. Weng, K. Chen, P. Ohresser, L. Nataf, F. Baudelet, Z. Sheng, S. Francoual, J. R. L. Mardegan, O. Leupold, Z. Li *et al.*, Phys. Rev. B **103**, 014414 (2021).

[17] Z. Liu, Q. Sun, X. Ye, X. Wang, L. Zhou, X. Shen, K. Chen, L. Nataf, F. Baudelet, S. Agrestini, C.-T. Chen, H.-J. Lin, H. B. Vasili, M. Valvidares, Z. Hu, Y.-f. Yang, and Y. Long, Appl. Phys. Lett. **117**, 152402 (2020).

[18] W. Kohn and L. J. Sham, Phys. Rev. **140**, A1133 (1965).

[19] P. E. Blöchl, Phys. Rev. B **50**, 17953 (1994).

[20] G. Kresse and D. Joubert, Phys. Rev. B **59**, 1758 (1999).

[21] G. Kresse and J. Furthmüller, Comput. Mater. Sci. **6**, 15 (1996).

[22] A. I. Liechtenstein, M. I. Katsnelson, V. P. Antropov, and V. A. Gubanov, J. Magn. Magn. Mater. **67**, 65 (1987).

[23] J. M. Wills, M. Alouani, P. Andersson, A. Delin, O. Eriksson, and O. Grechnyev, *Full-Potential Electronic Structure Method*, Vol. 167 (Springer, Berlin, Heidelberg, 2010).

[24] J. P. Perdew, K. Burke, and M. Ernzerhof, Phys. Rev. Lett. **77**, 3865 (1996).

[25] V. I. Anisimov, F. Aryasetiawan, and A. I. Lichtenstein, J. Phys.: Condens. Matter **9**, 767 (1997).

[26] S. L. Dudarev, G. A. Botton, S. Y. Savrasov, C. J. Humphreys, and A. P. Sutton, Phys. Rev. B **57**, 1505 (1998).

[27] O. Eriksson, A. Bergman, L. Bergqvist, and J. Hellsvik, *Atomistic Spin Dynamics: Foundations and Applications* (Oxford University Press, 2017).

[28] A. Ramirez, J. Phys.: Condens. Matter **9**, 8171 (1997).

[29] Z. Fang, K. Terakura, and J. Kanamori, Phys. Rev. B **63**, 180407(R) (2001).

[30] J. Kanamori and K. Terakura, J. Phys. Soc. Jpn. **70**, 1433 (2001).

[31] D. D. Sarma, P. Mahadevan, T. Saha-Dasgupta, S. Ray, and A. Kumar, Phys. Rev. Lett. **85**, 2549 (2000).

[32] L. Zhou, J. Dai, Y. Chai, H. Zhang, S. Dong, H. Cao, S. Calder, Y. Yin, X. Wang, X. Shen, Z. Liu, T. Saito, Y. Shimakawa, H. Hojo, Y. Ikuhara, M. Azuma, Z. Hu, Y. Sun, C. Jin, and Y. Long, Adv. Mater. **29**, 1703435 (2017).

[33] A. Belsky, M. Hellenbrandt, V. L. Karen, and P. Luksch, Acta Crystallographica Section B: Structural Science **58**, 364 (2002).

[34] See Supplemental Material at http://link.aps.org/supplemental/10.1103/PhysRevMaterials.5.054405 for the methodology of formation energy calculations, and calculated phonon spectrum, magnetization curves.

[35] A. R. Akbarzadeh, V. Ozoliņš, and C. Wolverton, Adv. Mater. **19**, 3233 (2007).

[36] M. Shaikh, A. Fathima, M. Swamynadhan, H. Das, and S. Ghosh, Chem. Mater. **33**, 1594 (2021).